Journal of Electroanalytical Chemistry 758 (2015) 125–134

Contents lists available at ScienceDirect

Journal of Electroanalytical Chemistry

journal homepage: www.elsevier.com/locate/jeac

Dynamic high potential treatment with dilute acids for lifting the capacitive performance of carbon nanotube/conducting polymer electrodes

Qin Yang [a], Siu-Kwong Pang [b,*], Kam-Chuen Yung [a]

[a] Department of Industrial and System Engineering, The Hong Kong Polytechnic University, Hung Hom, Kowloon, Hong Kong
[b] Institute of Textiles and Clothing, Faculty of Applied Science and Textiles, The Hong Kong Polytechnic University, Hung Hom, Kowloon, Hong Kong

ARTICLE INFO

Article history:
Received 8 July 2015
Received in revised form 16 October 2015
Accepted 21 October 2015
Available online 23 October 2015

Keywords:
Multiwalled carbon nanotubes
Poly-3,4-ethlyenedioxythiophene-polystyrene sulfonate
Dynamic high potential treatment
Supercapacitor electrodes

ABSTRACT

The capacitive behavior of the electrodes, fabricated from multiwalled carbon nanotubes (MWCNTs) and poly-3,4-ethlyenedioxythiophene–polystyrene sulfonate (PEDOT–PSS), before and after dynamic high potential treatment with dilute HNO_3 solutions, is investigated. The specific capacitance (C_{sp}) of the treated MWCNTs/PEDOT–PSS electrodes can be ~2.5 times higher than that of the untreated electrodes. The drop of C_{sp} in cycliability study for the treated electrodes is 0.8%, and much less than that for the untreated electrodes (16%). However, excessive treatment can deteriorate the capacitive performance of the electrodes. The morphology of MWCNTs/PEDOT–PSS composites revealed by transmission electron microscopy has no change after the treatment. The data of Raman spectroscopy show that the chemical structure of MWCNTs in the treated MWCNTs/PEDOT–PSS composites remains unchanged. The newly formed functional groups (COOH, C═O and S═O) are deemed to be generated by electrochemical oxidation of PEDOT, according to the X-ray photoelectron spectroscopy and Fourier transform infrared spectroscopy data. It is suggested that the C_{sp} of the treated MWCNTs/PEDOT–PSS electrodes is due to the interplay between two effects: 1) the degradation of PEDOT leads to the loss of capacitive characteristics; and 2) the newly formed functional groups in PEDOT in the treated electrodes result in the increase in the C_{sp}.

1. Introduction

Carbon nanotubes (CNTs), possessing the advantages of large specific surfaces, high conductivity, mechanical strength and chemical stability [1], are considered as promising material for supercapacitor electrodes. Pristine CNTs perform as a typical electric double layer capacitor (EDLC) during charge and discharge [2]. The larger surface area of pristine CNTs relative to other carbon materials can facilitate adsorption and desorption of abundant ions in the interface between the electrodes and electrolytes, leading to an increase in capacitance. However, since the capacitance of pristine CNTs is only contributed by simple physical adsorption of ions on the surface of CNTs, and the hydrophobicity of CNTs limits their electric capacity, the specific capacitance of pristine CNTs in aqueous electrolytes is not satisfactory [3].

Poly-3,4-ethlyenedioxythiophene-polystyrene sulfonate (PEDOT–PSS) is a mixture of polymers, PEDOT and PSS. PEDOT, a conducting polymer, contains a conjunction chain made of thiophene derivatives for electrical conduction [4], and it also has good thermal stability [5,6]. PEDOT–PSS is a promising material for supercapacitor electrodes because it can be used as a binder to fix CNTs onto substrates [3], and is an electroactive material that contributes pseudocapacitance to supercapacitors [7,8]. The specific capacitance of PEDOT–PSS varies in different electrolytes (0.02 F g^{-1} in Na_2SO_4 [9] and 10 F g^{-1} in $TBABF_4$/acetonitrile [10]). The drawback of conducting polymers is the poor cyclability because electrochemical degradation on the polymers causes decreases in both pseudocapacitance and conductivity [11].

In earlier publications, study of composites of carbon nanotubes and conducting polymers as supercapacitor electrodes has been reported [12–15]. Recently, some novel carbon-based materials, such as graphene paper, graphite sheets, mesoporous carbon and their composites, and doped carbon materials, have also been used to develop high performance supercapacitor electrodes [16–23]. Our team has investigated the composites of multiwalled carbon nanotubes (MWCNT) and PEDOT–PSS as supercapacitor electrodes in neutral aqueous solutions recently [3]. The advantage of composites is the possession of the merits of the two materials, and the aqueous solutions are safer and environmentally friendlier than organic solvents. In neutral aqueous electrolytes, the MWCNTs/5 wt.% PEDOT–PSS composite has the highest specific capacitance, while the MWCNTs/50 wt.% PEDOT–PSS composite can maintain the best capacitive behavior at higher scan rates. The pseudocapacitance of the MWCNTs/PEDOT–PSS composites decreases during continuous cycling due to the chemical degradation of PEDOT. The $-SO_3^-$ groups in PSS can retain the integrity during continuous

* Corresponding author.
E-mail address: pangsiukwong@gmail.com (S.-K. Pang).

http://dx.doi.org/10.1016/j.jelechem.2015.10.022
1572-6657/

cycling so they can still contribute to the capacitance of the composites through the ion adsorption and desorption in the electrical double layer [3].

In order to find a way to further increase the capacitance and the stability of the MWCNTs/PEDOT–PSS composites as supercapacitor electrodes in aqueous electrolytes, the performance of composites with and without treatment of dynamic high potentials in dilute acidic electrolytes was investigated. In addition, Raman spectroscopy, Fourier transform infrared spectroscopy (FTIR), X-ray Photoelectron Spectroscopy (XPS) and Transmission electron microscopy (TEM) were also used to characterize the MWCNTS/PEDOT–PSS composites before and after the dynamic high potential treatment.

2. Experimental

2.1. MWCNTs/PEDOT–PSS electrode fabrication

The fabrication of MWCNT/PEDOT–PSS electrodes was described previously [3]. Briefly, MWCNTs (length: 1–12 μm, outside diameter: 13–18 nm, purity: >99 wt.%, Cheap Tubes Inc., USA) and PEDOT–PSS (3.5 wt.% in solution, Aldrich, USA) with a mass ratio of 95:5 were dispersed in a mixture of ethanol and methanol (volume ratio of 4:1). The dispersion was subjected to 15 min of ultrasonic processing and then stirred overnight. A platinum plate, as a current collector, was covered with the dispersion of MWCNTs and PEDOT–PSS, and dried in an oven at 180 °C for 30 min to form the MWCNTs/PEDOT–PSS electrode.

2.2. Dynamic high potential treatment on MWCNTs/PEDOT–PSS electrodes

MWCNTs/PEDOT–PSS electrodes were treated with dynamic high potentials in a three-electrode system. A platinum wire and an Ag/AgCl electrode were used as a counter electrode and a reference electrode respectively. The treatment was conducted with a VersaSTAT potentiostat/galvanostat (Princeton Applied Research, USA). MWCNTs/PEDOT–PSS electrodes were immersed in HNO_3 solutions with different concentrations of 0.05 M, 0.1 M, 0.2 M and 0.5 M, and the potential was continuously cycled from 1 V to 2 V at a scan rate of 50 mV s^{-1}. Fig. 1 shows the CV curves of MWCNTs/PEDOT–PSS electrodes in HNO_3 solutions during dynamic high potential treatment, and Fig. 1 insert is the schematic representation of dynamic high potential treatment.

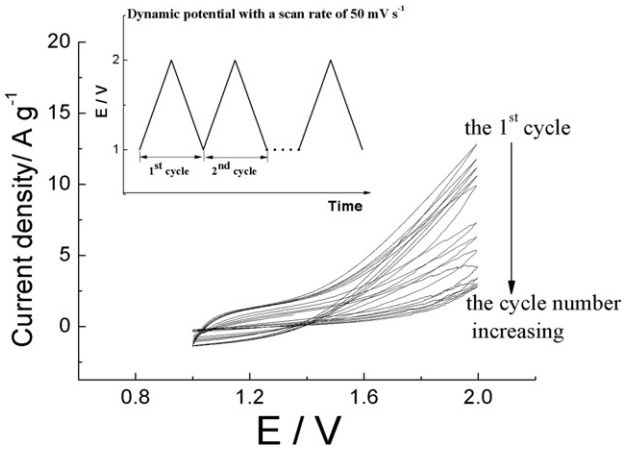

Fig. 1. The CV curves describing the dynamic high potential treatment on MWCNTs/PEDOT–PSS electrodes in HNO_3 solutions, and schematic representation of dynamic high potential treatment (insert).

2.3. Electrochemical measurements

Cyclic voltammetry (CV) and electrochemical impedance spectroscopy (EIS) were conducted to evaluate the electrochemical performance of the MWCNTs/PEDOT–PSS electrodes. All the electrochemical measurements were carried out using a VersSTAT 3 potentiostat/galvanostat (Princeton Applied Research, USA). A pure platinum wire as a counter electrode and an Ag/AgCl electrode as a reference electrode were employed. The EIS frequency ranged from 100 kHz to 0.1 Hz, and an ac amplitude of 5 mV, superimposed on a dc voltage of 0.4 V (the middle value of the operating potential window: 0 V–0.8 V described in the CVs shown in Figs. 1 and 2), was applied. All the electrochemical measurements were conducted in 1 M HNO_3.

2.4. Transmission electron microscopy characterization

The morphology of the MWCNTs/PEDOT–PSS composites was characterized by transmission electron microscopy (TEM, JEOL JEM-2011). The samples were dispersed in ethanol with 10 min of ultrasonic vibration. The dispersion was placed on a holey-carbon coated copper gird, and dried in the oven at 60 °C for 5 min.

2.5. Raman spectroscopy measurement

Raman spectra of the MWCNTs/PEDOT–PSS composites were recorded on a MicroRaman/Photoluminescence spectrometer (Renishaw InVia) equipped with a 633 nm Ar ion laser.

2.6. X-ray photoelectron spectrometry measurement

X-ray Photoelectron spectroscopy measurements on the MWCNTs/PEDOT–PSS composites were carried out by an Axis Ultra DLD X-ray photoelectron spectrometer (Kratos). The Al K X-ray source was used, and the binding energy was collected and calibrated using the C 1 s peak at 284.5 eV.

2.7. Fourier transform infrared spectroscopy measurement

The MWCNTs/PEDOT–PSS composites were mixed with KBr powder and pressed to form pellets for subsequent FTIR measurements. FTIR spectra were obtained using a Spectrum 100 FTIR spectrometer (PekinElmer).

3. Results and discussion

3.1. Electrochemical performance of the MWCNTs/PEDOT–PSS electrodes before and after dynamic high potential treatment

3.1.1. Cyclic voltammetry measurements

Fig. 2 shows the cyclic voltammetry (CV) curves of the MWCNTs/PEDOT–PSS electrodes before and after the dynamic high potential treatment with different concentrations of HNO_3 solutions and various cycles. Before the treatment, a couple of redox reactions occurred in PEDOT at ~0.7 V in the forward and backward scans. The location of this pair of redox reaction peaks (~0.7 V) in acidic solutions is somewhat different from that in neutral solutions (~0.55 V) [3]. There were another couple of redox reactions that happened in PEDOT at ~0.5 V in the forward scan and ~0.1 V in the backward scan. After the treatment, only a pair of broad redox peaks at ~0.45 V in the forward scan and ~0.3 V in the backward scan of the CV curves of the MWCNTs/PEDOT–PSS electrodes was observed (Fig. 2). Also, the treatment caused a significant increase in the capacitance of the MWCNTs/PEDOT–PSS electrodes. However, when the number of treatment cycles increased to certain values (40th cycle in 0.05 M HNO_3; 20th cycle in 0.1 M HNO_3; 10th cycle in 0.2 M HNO_3; 5th cycle in 0.5 M HNO_3), the CV curves of the MWCNTs/PEDOT–PSS electrodes changed to a spindle

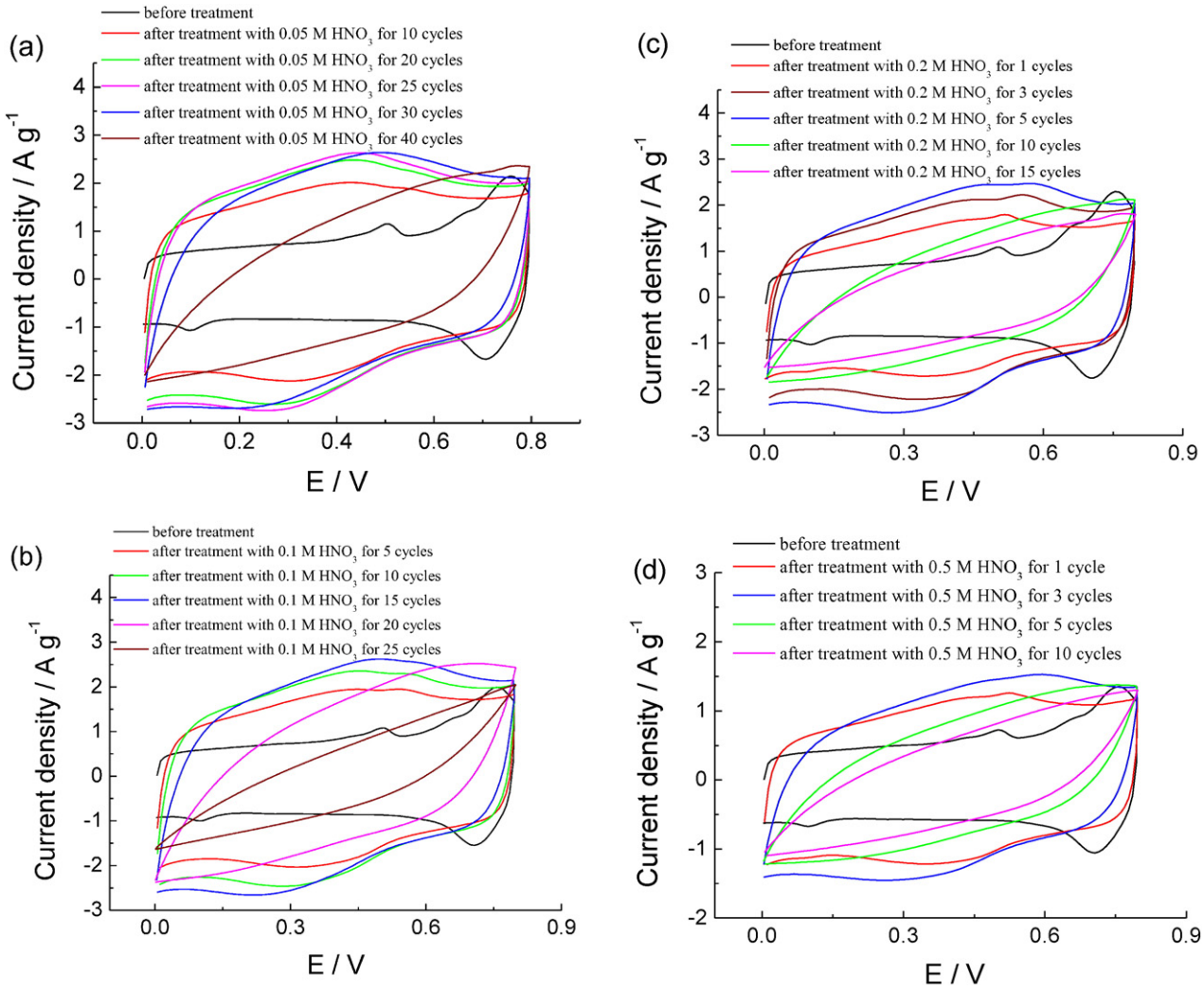

Fig. 2. Cyclic voltammograms of the MWCNTs/PEDOT–PSS electrodes in 1 M HNO_3 with a scan rate of 50 mV s^{-1}, obtained using an Ag/AgCl reference electrode, before and after the dynamic high potential treatment with (a) 0.05 M; (b) 0.1 M; (c) 0.2 M; (d) 0.5 M HNO_3 for various cycles.

shape from a quasi-rectangle shape. It means that the MWCNTs/PEDOT–PSS electrodes lose their capacitive characteristics after excessive treatment.

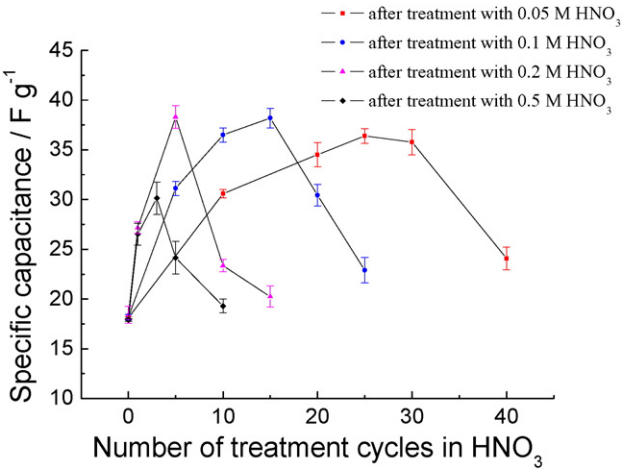

Fig. 3. The specific capacitance of the MWCNTs/PEDOT–PSS electrodes as a function of the number of the dynamic high potential treatment cycles.

3.1.2. Effects of treatment cycle

The specific capacitance of the MWCNTs/PEDOT–PSS electrodes was calculated from the CV curves using the following Eq. (1) [3,24]:

$$C_{sp} = \frac{1}{mv(V_2 - V_1)} \int_{V_1}^{V_2} I(V)dV \quad (1)$$

where C_{sp} is the specific capacitance (F g^{-1}), v is the potential scan rate (V s^{-1}), V_1, V_2 are switching potentials in cyclic voltammetry (V), and I (V) denotes the response current (A).

Fig. 3 shows the specific capacitance of the MWCNTs/PEDOT–PSS electrodes subjected to the dynamic high potential treatment with different HNO_3 concentrations (0.05 M, 0.1 M, 0.2 M, 0.5 M), as a function of the number of treatment cycles. From Fig. 3, the specific capacitance of the MWCNTs/PEDOT–PSS electrodes before treatment is ~18 F g^{-1}, and increase to optimum values: ~36 F g^{-1}, ~38 F g^{-1}, ~38 F g^{-1} and ~30 F g^{-1} after the treatment with 0.05 M HNO_3 for 25 cycles, 0.1 M HNO_3 for 15 cycles, 0.2 M HNO_3 for 5 cycles and 0.5 M HNO_3 for 3 cycles respectively. From the previous study, the specific capacitance of PEDOT–PSS in Na_2SO_4 is only 0.02 F g^{-1} [9]. When combining with MWCNTs, the specific capacitance of the MWCNTs/PEDOT–PSS composite can reach 12 F g^{-1} in Na_2SO_4 [3]. In this study, the specific capacitance of MWCNTs/PEDOT–PSS after the treatment can be enhanced to 38 F g^{-1}, around two times higher than the untreated MWCNTs/PEDOT–PSS electrode (18 F g^{-1}). The improvement of specific

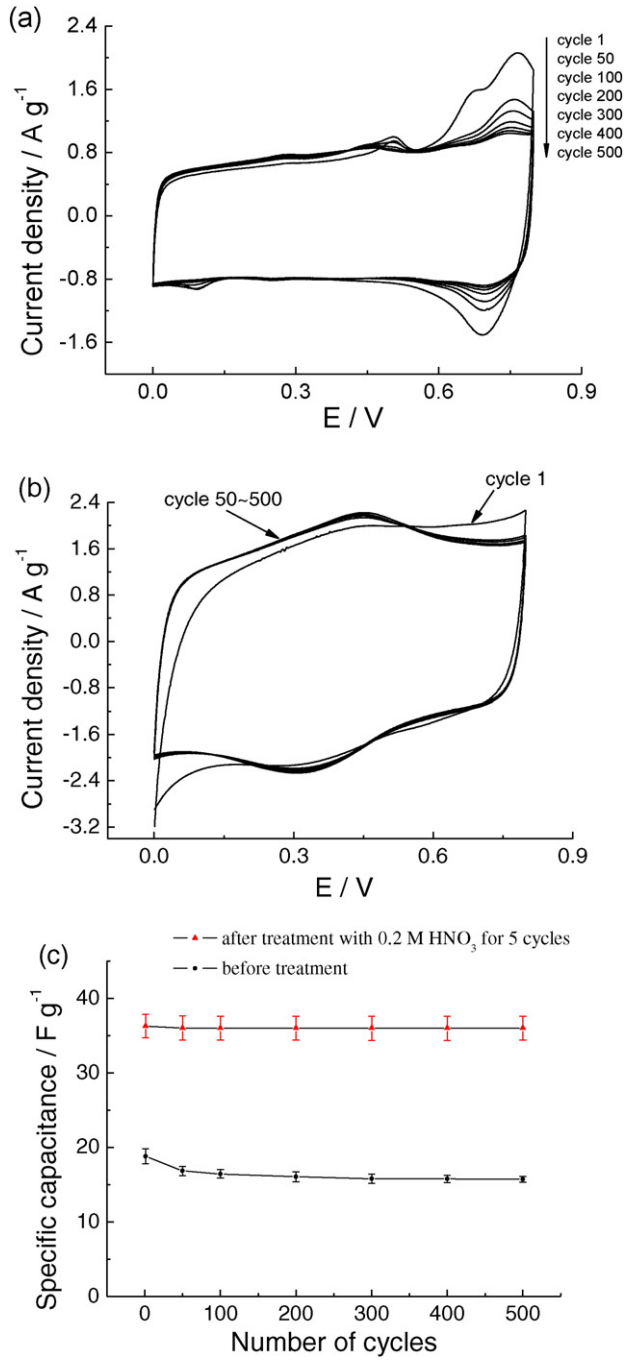

Fig. 4. Cyclic voltammograms of the MWCNTs/PEDOT–PSS electrodes in 1 M HNO_3 with a scan rate of 50 mV s^{-1}, obtained using an Ag/AgCl reference electrode, (a) before and (b) after the 5-cycle dynamic high potential treatment with 0.2 M HNO_3. (c) Cyclability of the treated and untreated MWCNTs/PEDOT–PSS electrodes.

capacitance of the treated electrodes may result from the formation of polar functional groups in PEDOT in the MWCNTs/PEDOT–PSS composites, and it will be discussed in Sections 3.4 and 3.5. Further increase in the number of cycles causes the specific capacitance to decline dramatically because of the loss of the capacitance characteristics (Fig. 2). Such loss of the capacitance characteristics after excessive treatment may be attributed to the severe electrochemical degradation of PEDOT–PSS, which leads to an increase in the equivalent series resistance (ESR) of the MWCNTs/PEDOT–PSS electrodes. The increase in the equivalent series resistance will be elaborated with the electrochemical impedance data in Section 3.1.5, the XPS spectra in Section 3.4 and the FTIR spectra in Section 3.5.

From Fig. 3, the dynamic high potential treatment with dilute acids can further improve the specific capacitance of MWCNTs/PEDOT–PSS electrodes in acidic solutions. Also, the 15-cycle dynamic high potential treatment with 0.1 M HNO_3 and the 5-cycle dynamic high potential treatment with 0.2 M HNO_3 can attain the same and optimal specific capacitance. Herein, the treatment with 0.2 M HNO_3 for 5 cycles was chosen in the cyclability study (Section 3.1.5) and other characterization study (Sections 3.2–3.5).

3.1.3. Cyclability

Fig. 4 shows the cyclability of the MWCNTs/PEDOT–PSS electrodes before and after the dynamic high potential treatment with 0.2 M HNO_3 for 5 cycles. For the untreated MWCNTs/PEDOT–PSS electrodes, the redox peaks at ~0.7 V diminish with increasing CV cycles (Fig. 4a), and it reflects the gradual electrochemical degradation of the PEDOT–PSS in the untreated MWCNTs/PEDOT–PSS composites during cycling, and causing a 16% (3 F g^{-1}) drop of specific capacitance in the first 300 cycles (Fig. 4c). In addition, the specific capacitance of the untreated MWCNTs/PEDOT–PSS electrodes becomes stable after 100 CV cycles. After the 5-cycle dynamic high potential treatment with 0.2 M HNO_3 (conditions for achieving the optimum specific capacitance according to Fig. 3), the pair of broad redox peaks at ~0.45 V in the forward scan and ~0.3 V in the backward scan in nitric acid solutions can remain stable over 500 CV cycles (Fig. 4b), and only a 0.8% (0.3 F g^{-1}) drop in specific capacitance in the first 300 cycles was observed (Fig. 4c); therefore there is almost no change in the specific capacitance of the treated MWCNTs/PEDOT–PSS electrodes for 500 CV cycles (Fig. 4c). This pair of highly reversible broad redox peaks at ~0.45 V may be attributed to the newly formed functional groups in PEDOT in the treated MWCNTs/PEDOT–PSS electrodes, and this electrochemically modified structure of PEDOT in the treated MWCNTs/PEDOT–PSS electrodes in nitric acid solutions shows to be more stable in the cyclability test than the original structure of PEDOT in the untreated MWCNTs/PEDOT–PSS electrodes.

Table 1 shows the C_{sp} and the drop of C_{sp} for the MWCNTs/PEDOT–PSS electrodes with and without the dynamic high potential treatment in dilute acidic solutions. The C_{sp} of the treated MWCNTs/PEDOT–PSS electrodes (38 ± 1.62 F g^{-1}; triplicate) is ~2.5 times significantly higher than that of the untreated electrodes (16 ± 0.63 F g^{-1}; triplicate) at the 300th cycle because of the newly formed polar functional groups in PEDOT in the treated MWCNTs/PEDOT–PSS electrodes. The characterization of these newly formed polar functional groups in PEDOT will be discussed in Sections 3.4 and 3.5.

According to our previous study, the C_{sp} of the MWCNTS/PEDOT–PSS electrodes in neutral solutions is 12 ± 0.5 F g^{-1} (triplicate), and the drop of C_{sp} in the first 300 cycles is 23% [3]. In the current study, the C_{sp} of the MWCNTs/PEDOT–PSS electrodes operating in acids is 16 ± 0.63 F g^{-1} (triplicate), which is 1.4 times significantly higher than that in neutral solutions, and the drop of C_{sp} in acids is only 16% (Fig. 3a). Furthermore, the C_{sp} and the stability of the treated MWCNTs/PEDOT–PSS electrodes operating in acids (38 ± 1.62 F g^{-1}; 0.8% drop in the first 300 cycles) is

Table 1
C_{sp} and its drop of MWCNTs/PEDOT–PSS electrodes with and without treatment in different electrolytes, measured at a scan rate of 50 mV/s.

Electrode treatment	Electrolyte	C_{sp} after 300 cycles (F g^{-1})	Drop of C_{sp} at the 300th cycle
NA	1 M Na_2SO_4	12 ± 0.5 [3]	23%
NA	1 M HNO_3	16 ± 0.63	16%
Dynamic high potentials in acid	1 M HNO_3	38 ± 1.62	0.8%

significantly greater than those in neutral solutions (12 ± 0.5 F g^{-1}; 23% drop in the first 300 cycles). Thus, the MWCNTs/PEDOT–PSS electrodes can achieve higher stability and specific capacitance in acidic electrolytes relative to neutral solutions, and they can be improved further after the dynamic high potential treatment with dilute acids.

3.1.4. Scan-rate dependent cyclic voltammetry

The rate-dependent CV curves of the MWCNTs/PEDOT–PSS electrodes before and after dynamic high potential treatment were measured in 1 M HNO_3. The rectangular-shaped CV curves can be distorted at higher scan rates because of the ionic diffusion limitation [25], and the equivalent series resistance (ESR) also affects the scan rate-dependent CV curves [26]. The CV curves of the untreated MWCNTs/PEDOT–PSS electrodes and the MWCNTs/PEDOT–PSS electrodes subjected to the treatment with 0.2 M HNO_3 for 3 cycles can retain a quasi-rectangular shape when the scan rate increases from 10 mV s^{-1} to 400 mV s^{-1} (Fig. 5a–e). This means that they can preserve capacitive characteristics up to a scan rate of 400 mV s^{-1}. When the

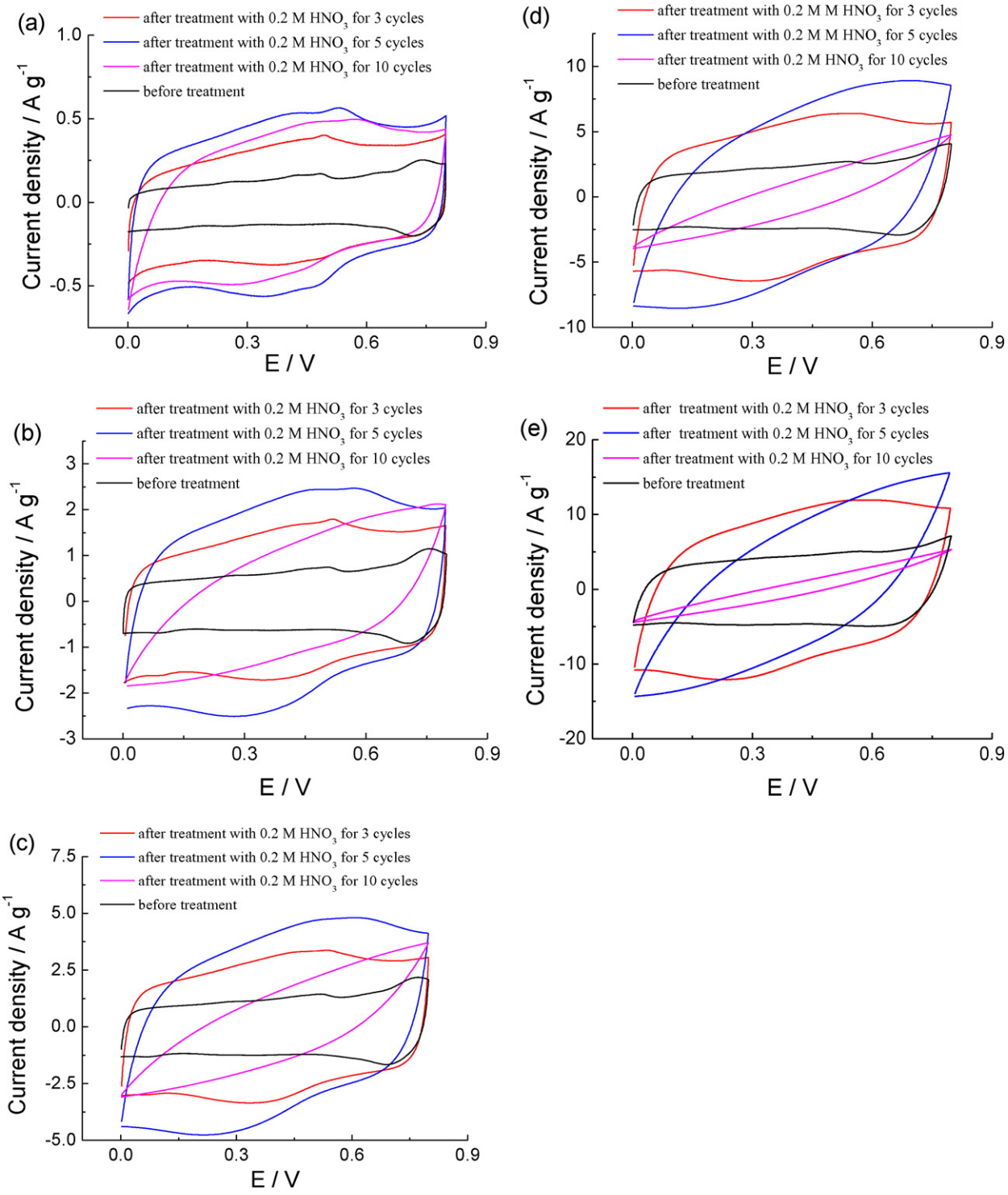

Fig. 5. Cyclic voltammograms of the MWCNTs/PEDOT–PSS electrodes before and after the dynamic high potential treatment (0.2 M HNO_3; 3 cycles, 5 cycles and 10 cycles) at diverse scan rates: (a) 10 mV s^{-1}; (b) 50 mV s^{-1}; (c) 100 mV s^{-1}; (d) 200 mV s^{-1}; (e) 400 mV s^{-1} in 1 M HNO_3 solutions, obtained using an Ag/AgCl reference electrode.

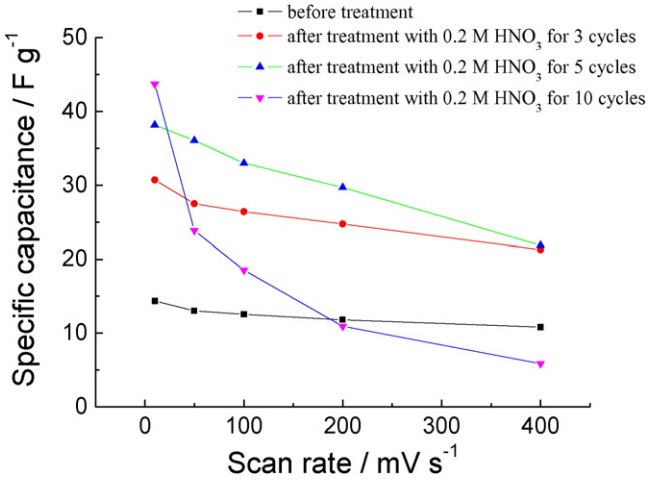

Fig. 6. The specific capacitance of the MWCNTs/PEDOT–PSS electrodes before and after the dynamic high potential treatment (0.2 M HNO_3; 3 cycles, 5 cycles and 10 cycles) under various scan rates (10 mV s^{-1}, 50 mV s^{-1}, 100 mV s^{-1}, 200 mV s^{-1}, 400 mV s^{-1}).

treatment cycle increases to 5, the CV curves of the treated MWCNTs/PEDOT–PSS electrodes become slightly distorted from a quasi-rectangular shape when the scan rate rises to 200 mV s^{-1} (Fig. 5d), and are severely deformed to a spindle shape at a scan rate of 400 mV s^{-1} (Fig. 5e). After 10 cycles of the treatment, the MWCNTs/PEDOT–PSS electrodes lose their quasi-rectangular CV curves at the scan rate of 10 mV s^{-1} or higher (Fig. 5b-e). The results reflect that the greater number of the treatment cycles makes the MWCNTs/PEDOT–PSS electrodes difficultly maintain the capacitive characteristics at higher scan rates. This may be attributed to a large number of treatment cycles leading to more severe electrochemical degradation of PEDOT–PSS, hence higher ESR of the MWCNTs/PEDOT–PSS electrodes results. The higher ESR of MWCNTs/PEDOT–PSS electrodes caused by more treatment cycles can also be demonstrated with the electrochemical impedance results shown in Section 3.1.5.

Fig. 6 shows the specific capacitance of the MWCNTs/PEDOT–PSS electrodes with and without the dynamic high potential treatment, as a function of the scan rate. When comparing with the treated electrodes, the untreated electrodes express a minor drop at higher scan rates. However, the specific capacitance of the treated electrodes decreases rapidly with increasing the scan rate, and this drop of specific capacitance becomes severe when the number of treatment cycles increases. It may be attributed that the treatment raises the ESR of the MWCNTs/PEDOT–PSS electrodes, which is revealed by the electrochemical impedance data in Section 3.1.5.

3.1.5. Electrochemical impedance

Nyquist plots of the MWCNTs/PEDOT–PSS electrodes, before and after the dynamic high potential treatment with 0.2 M HNO_3 for different cycles, are depicted in Fig. 7a. The Nyquist plots consist of semicircles in high frequency regions (Fig. 7a insert) and quasi-vertical lines in low frequency regions (Fig. 7a). At the high frequency intercepts on the real axis show an internal resistance including the resistance of the electrolytes, electrode materials and the contact resistance between the electrode materials and the current collector [27]. The quasi-vertical lines in the low frequency range reflect that the treated and untreated MWCNTs/PEDOT–PSS electrodes possess capacitive characteristics [28]. The diameters of the semicircles corresponding to the charge transfer resistance (R_{ct}) [29] in the medium frequency range for the MWCNTs/PEDOT–PSS electrodes increase with the number of the treatment cycles. It can be explained by the electrochemical degradation of PEDOT after the repeated treatment, reducing the rates of faradic reactions at PEDOT.

The imaginary capacitances of the electrodes before and after the treatment as a function of frequency are plotted in Fig. 7b. The time constants τ were calculated from the frequencies f_0 ($\tau = (2\pi f_0)^{-1}$) at which the imaginary capacitance reaches the maximum values [30]. According to Fig. 7b, the frequencies f_0 decrease when the electrodes are subjected to more cycles of the treatment. In turn, the calculated time constants τ increase with the treatment cycles: 0.08 s before treatment; 0.32 s after treatment for 5 cycles; 0.64 s after treatment for 10 cycles and 1.27 s after treatment for 15 cycles. Shorter time constants mean quicker faradic processes [31,32], so rates of faradic reactions at electrodes decrease with increasing treatment cycles. The conduction mechanism of PEDOT–PSS involves the faradic reactions at the PEDOT backbone [33], the depression of the PEDOT faradic reaction rates caused by repeated treatment can lower the conductivity of PEDOT–PSS. Hence, the ESR of the MWCNTs/PEDOT–PSS electrodes becomes higher.

3.2. Transmission electron microscopy characterization

Fig. 8 shows the TEM images of the structure of MWCNT in the MWCNTs/PEDOT–PSS composites before (Fig. 8a) and after the dynamic high potential treatment with 0.2 M HNO_3 for 5 cycles (Fig. 8b) and 15 cycles (Fig. 8c). The structures of MWCNTs in the treated MWCNTs/PEDOT–PSS composites can maintain the integrity, and no defects on the sidewalls of MWCNTs appear after the treatment. It implies that the repeated treatment with cycling from 1 V to 2 V in dilute nitric acid solutions cannot damage the structure of MWCNTs in the MWCNTs/PEDOT–PSS composites.

3.3. Raman spectroscopy analysis

Fig. 9 shows the Raman spectra of the pristine MWCNTs and the MWCNTs/PEDOT–PSS composites before and after the dynamic high potential treatment with 0.2 M HNO_3 for 5 cycles and 15 cycles. The spectra were normalized to the D band. The typical Raman features of MWCNTs including the D band (~1340 cm^{-1}), G band (~1580 cm^{-1}) and D′ band (~1620 cm^{-1}) [34] were revealed when the MWCNTs, and the treated and untreated MWCNTs/PEDOT–PSS composites, were characterized. Amorphous carbon and structural defects in MWCNTs result in the D band, and the G band originates from the tangential in-plane stretching of C═C bonds [35]. The D′ band on the stretching of G band corresponds to the defects on the sidewalls of MWCNTs [36]. The D/G ratios of the MWCNTs/PEDOT–PSS composites, before and after the treatment, are almost the same. These results indicate that the surfaces of MWCNTs in the MWCNTs/PEDOT–PSS composites keep unchanged after the treatment, and there are no additional functional groups such as carbonyl, carboxyl or hydroxyl forming on the surfaces of MWCNTs during the treatment. Unlike the oxidation of MWCNTs in thermal acids with high concentrations reported in other papers (>60 wt.%, ~16 M) [37,38], the dynamic potential treatment in dilute HNO_3 with a low concentration (0.2 M) cannot induce any chemical changes on the MWCNT surfaces. Therefore, the MWCNTs in the MWCNTs/PEDOT–PSS composites remain chemically unchanged during the repeated treatment, with cycling from 1 V to 2 V, in dilute nitric acid solutions.

3.4. X-ray photoelectron spectroscopy analysis

The XPS spectra of the pristine MWCNTs and the MWCNTs/PEDOT–PSS composites before and after the dynamic high potential treatment with 0.2 M HNO_3 for 5 cycles and 15 cycles are displaced in Fig. 10.

The main peaks in the C 1 s spectra are observed at 284.5 eV (Fig. 10a), and they originate from the carbon atoms in the sp^2-hybridized graphitic structure of MWCNTs and the carbon atoms binding to hydrogen atoms in PEDOT–PSS [1,39]. The peaks in the range from 286 eV to 290 eV correspond to the carbon atoms bonding to oxygen atoms [40,41]. The insert in Fig. 10a shows the signals ranging from 286 eV to 290 eV for the

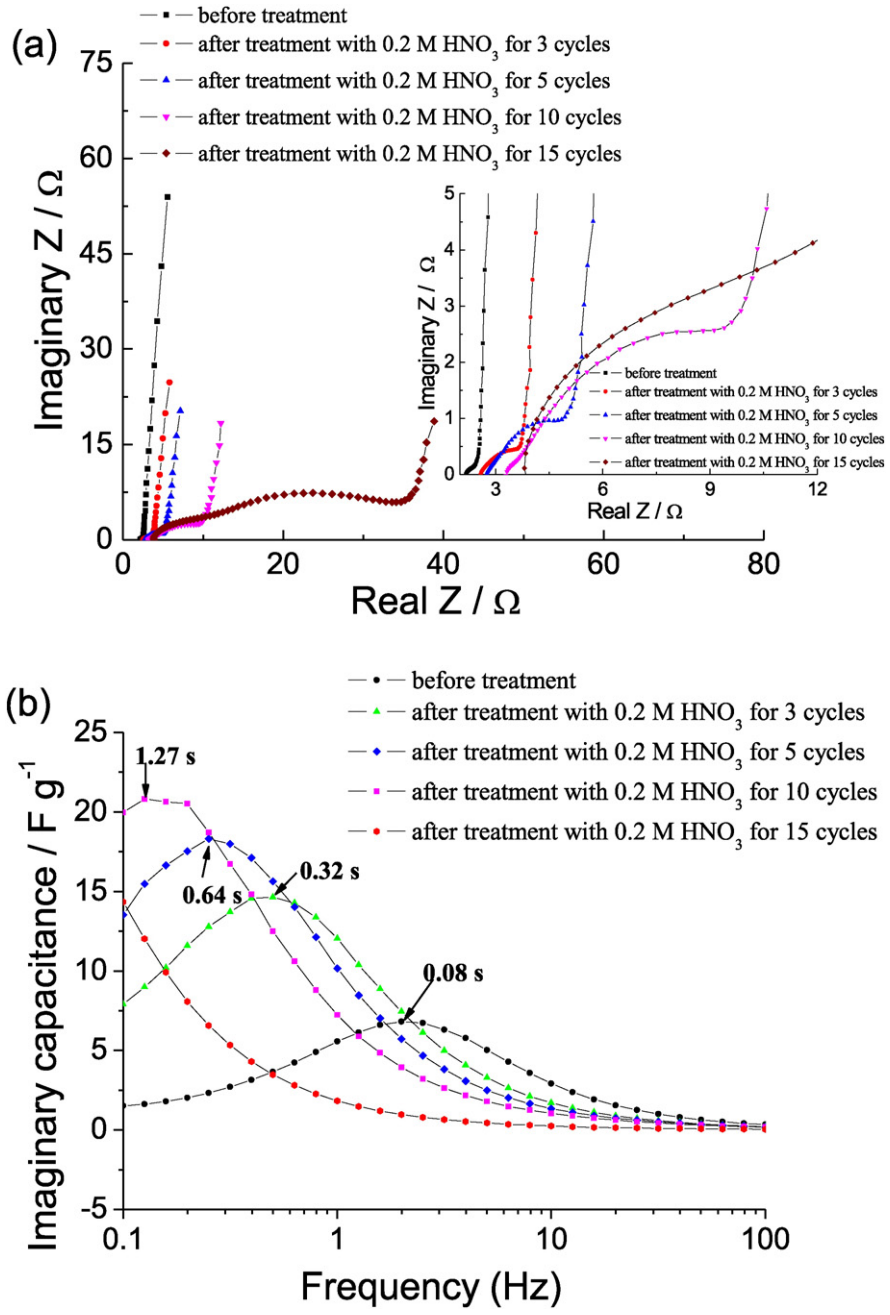

Fig. 7. (a) Nyquist plots of the MWCNTs/PEDOT–PSS electrodes after the treatment with 0.2 M HNO_3 for different cycles, at 5 mV (ac) superimposed on 0.4 V (dc) vs. Ag/AgCl with frequencies that ranged from 100 kHz to 0.1 Hz, measured in 1 M HNO_3 solutions; (b) Evolution of imaginary capacitance of the MWCNTs/PEDOT–PSS electrodes before and after the treatment vs. frequency, where the calculated characteristic time constants τ are indicated.

treated and untreated MWCNTs/PEDOT–PSS composites, and they can be assigned to the C–O–C, the C–OH and the C═O in PEDOT generated by the treatment.

From Fig. 10b, depicting the O 1 s spectra, the strong broad peaks for the MWCNTs/PEDOT–PSS composites contain two main features: the signal at 532 eV attributed to the oxygen atoms in the sulfonic groups in PSS, and the peak at 533.4 eV resulting from the oxygen atoms binding to carbon atoms in PEDOT [39]. The ratios of the intensity of the peak at 533.4 eV to the peak intensity at 532 eV for the treated MWCNTs/PEDOT–PSS composites are higher than the corresponding ratio for the untreated MWCNTs/PEDOT–PSS composites. It can be explained by more C–OH and C═O groups being produced during the treatment. According to the Raman results, there is no chemical change in MWCNTs in the MWCNTs/PEDOT–PSS composites during the treatment; therefore, the newly formed functional groups (C–OH and C═O) are deemed to be generated by the oxidation of PEDOT.

The S 2p spectra are depicted in Fig. 10c. A peak at 168.8 eV is ascribed to the S atoms in S–O/S═O in PSS [42,43]. The two peaks at 163.8 eV (S $2p_{1/2}$) and 165.2 eV (S $2p_{3/2}$), which are attributed to the S atoms in C–S–C [42,43] in PEDOT in the untreated MWCNTs/PEDOT–PSS composites. For the treated MWCNTs/PEDOT–PSS composites, the two peaks at 163.8 eV and 165.2 eV disappear. It is suggested that the S atoms in PEDOT are oxidized to S–O/S═O during the treatment.

3.5. Fourier transform infrared spectroscopy analysis

The FTIR was conducted to identify the functional groups on the pristine MWCNTs and the MWCNTs/PEDOT–PSS composites before and

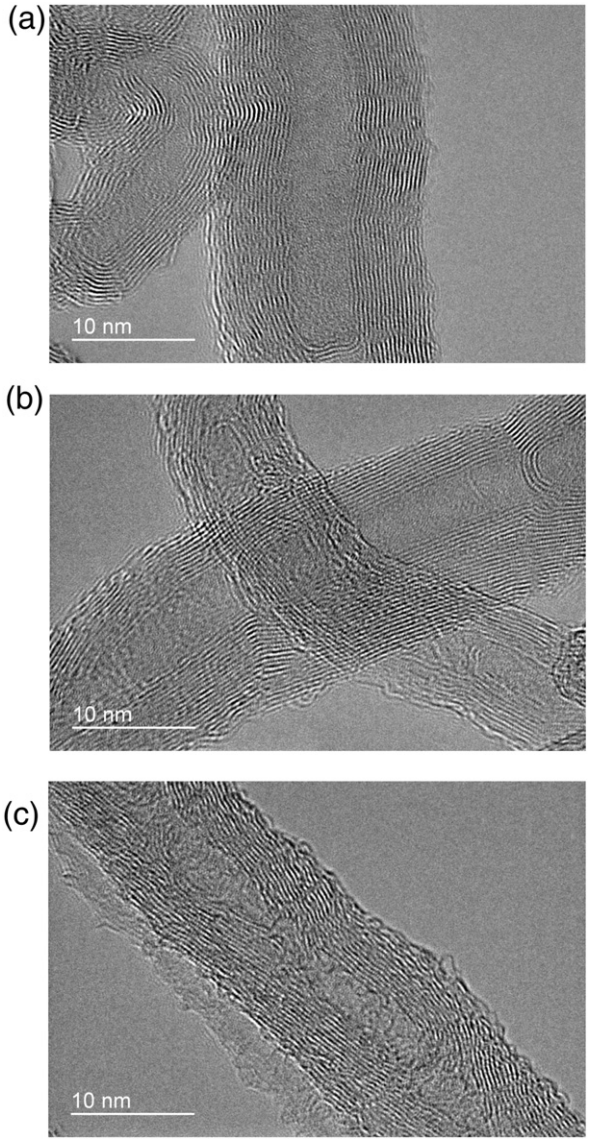

Fig. 8. TEM images of the structure of MWCNTs in MWCNTs/PEDOT–PSS composites before (a) and after the dynamic high potential treatment with 0.2 M HNO_3 for 5 cycles (b) and 15 cycles (c).

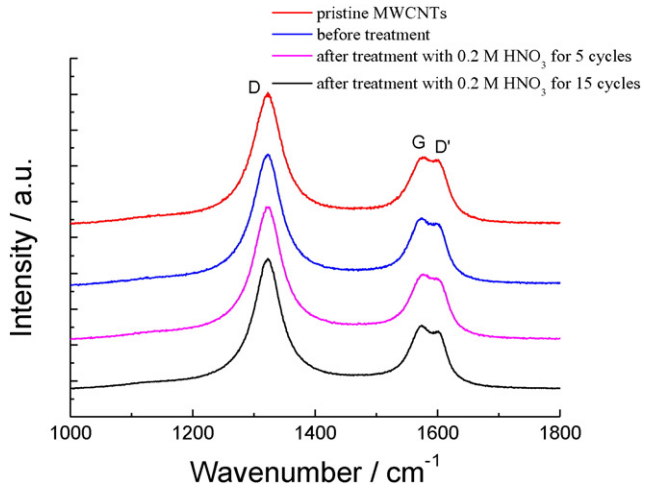

Fig. 9. Raman spectra of the pristine MWCNTs and the MWCNTs/PEDOT–PSS composites before and after the dynamic high potential treatment with 0.2 M HNO_3 for 5 cycles and 15 cycles.

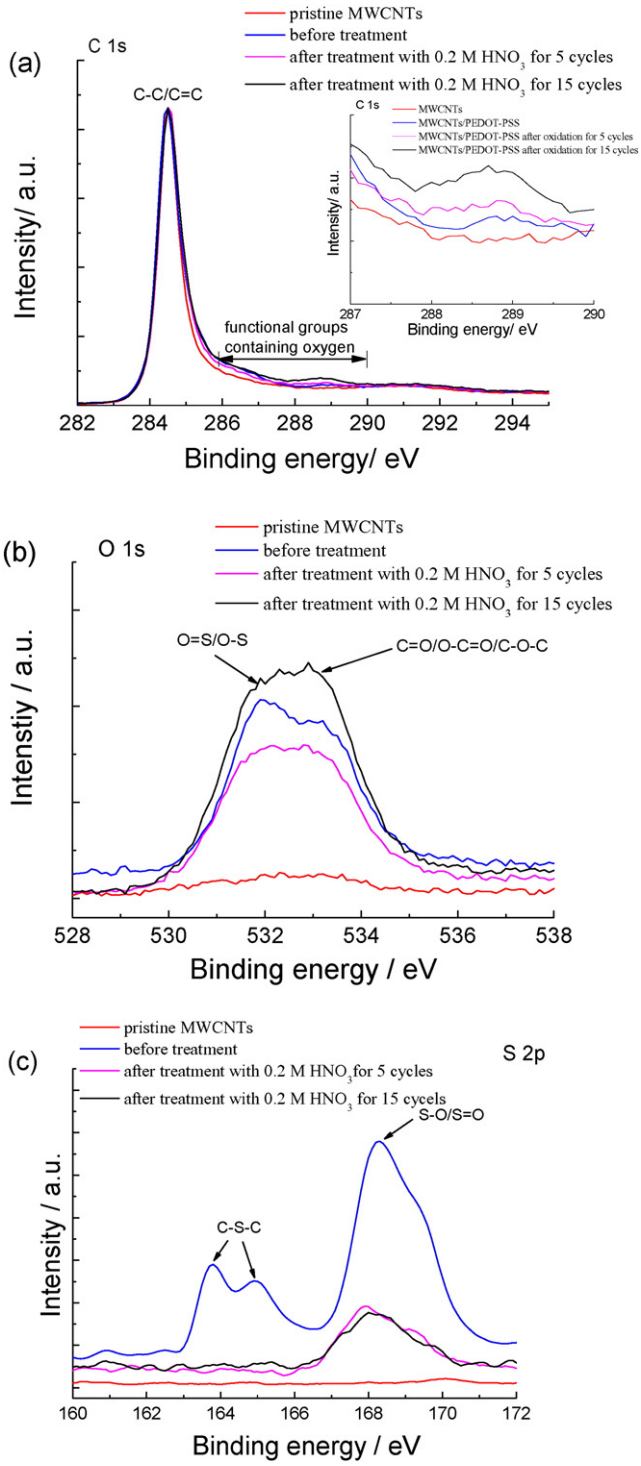

Fig. 10. The XPS spectra of (a) C 1 s, (b) O 1 s and (c) S 2 p for pristine MWCNTs and the MWCNTs/PEDOT–PSS composites before and after the dynamic high potential treatment with 0.2 M HNO_3 for 5 and 15 cycles.

after the dynamic high potential treatment with 0.2 M HNO_3 for 5 and 15 cycles. The MWCNTs in the MWCNTs/PEDOT–PSS composites remain chemically unchanged during the treatment according to the Raman data, so the chemical changes observed in the FTIR spectra occur in PEDOT–PSS (Fig. 11). From Fig. 11, the two broad peaks at 1720 cm^{-1} and 1580 cm^{-1}, assigned to the C═O stretching from COOH groups [44] and C═O groups respectively, are observed for the treated MWCNTs/PEDOT–PSS composites, but these two peaks do not appear for the untreated MWCNTs/PEDOT–PSS composites. It is

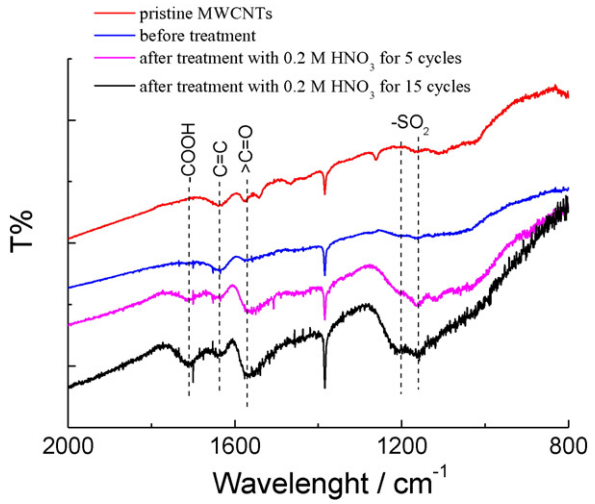

Fig. 11. FTIR spectra of pristine MWCNTs and the MWCNTs/PEDOT–PSS composites before and after the dynamic high potential treatment with 0.2 M HNO_3 for 5 cycles and 15 cycles.

suggested that the carbon atoms in PEDOT are electrochemically oxidized to form COOH and C═O during the treatment [39]. The peak at 1640 cm^{-1} originates from the C═C stretching [40,45]. The broad peak in the range from 1050 cm^{-1} to 1200 cm^{-1} is assigned to the $S(=O)_2$ stretching [39], and its intensity after treatment is larger than before the treatment. It can be explained by the S atoms in C–S–C in PEDOT being oxidized to form S═O during the treatment.

3.6. Mechanisms of lifting the capacitive performance

Fig. 12 shows the schematic of introducing newly formed polar functional groups (COOH, C═O, and S═O) in PEDOT after the high dynamic potential treatment with dilute acids. These polar functional groups in the treated MWCNT/PEDOT–PSS composites contribute to the faradic processes during charge and discharge (CV curves on the right of Fig. 12) compared with the untreated composites (CV curves on the left of Fig. 12), exerting pseudo-capacitance on the treated electrodes. In addition, the newly formed polar functional groups can provide more active sites to adsorb more ions from electrolytes on the electrodes, hence increase the electrostatic double-layer capacitance of the treated MWCNTs/PEDOT–PSS electrodes relative to the untreated ones.

4. Conclusions

The specific capacitance of the MWCNTs/PEDOT–PSS electrodes operated in acids is 1.4 times higher than that in neutral solutions. After the dynamic high potential treatment with dilute nitric acid solutions for appropriate cycles, the specific capacitance can be elevated further, and the optimum specific capacitance is ~2.5 times higher than the specific capacitance without treatment. The cyclability of the electrodes after the optimum treatment is better than the electrodes without the treatment. Also, the cyclability for operation in acids is superior to that in neutral solutions. However, the specific capacitance decreases by increasing the number of treatment cycles because of the loss of the capacitive characteristics (spindle-shaped CV curves). The larger number of the treatment cycles also causes the MWCNTs/PEDOT–PSS electrodes to lose their capacitive characteristics more easily at higher rates of charge and discharge.

According to the results of TEM and Raman spectroscopy, the morphology of the MWCNTs/PEDOT–PSS composites and the chemical structure of MWCNTs in the MWCNTs/PEDOT–PSS composites remain unchanged respectively after the treatment. The XPS and FTIR data reveal that the treatment causes the formation of polar functional groups COOH, C═O and S═O in PEDOT. It is suggested that these newly formed functional groups in PEDOT reflect the damage to the original conjunction path in PEDOT by electrochemical oxidation (chemical degradation of PEDOT) during the treatment, leading to the larger R_{ct} and hence the greater ESR of the treated MWCNTs/PEDOT–PSS electrodes. On the other hand, these polar functional groups in PEDOT in the treated MWCNTs/PEDOT–PSS electrodes provide more active sites to adsorb more ions from electrolytes on the electrodes, resulting in the higher specific capacitance, when compared with the untreated MWCNTs/PEDOT–PSS electrodes. Therefore, achieving an optimum specific capacitance is due to the interplay between these two effects produced by the formation of the aforementioned polar functional groups in PEDOT.

Acknowledgements

The work described in this paper was supported by the Research Committee of The Hong Kong Polytechnic University under the project

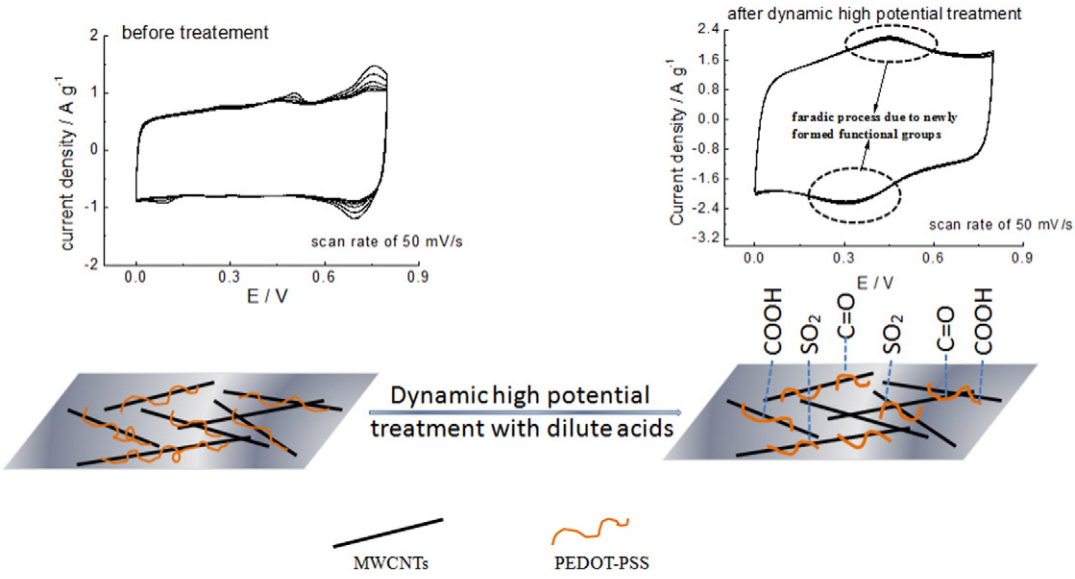

Fig. 12. Schematic of MWCNTs/PEDOT–PSS before and after the dynamic high potential treatment with dilute acids, and their corresponding electrochemical performance.

No. RTAP. The authors thank the Materials Characterization and Device Fabrication Center in The Hong Kong Polytechnic University for Electron Microscopy scanning.

References

[1] G. Moraitis, Z. Špitalský, F. Ravani, A. Siokou, C. Galiotis, Electrochemical oxidation of multi-wall carbon nanotubes, Carbon 49 (2011) 2702–2708.
[2] C. Peng, S. Zhang, D. Jewell, G.Z. Chen, Carbon nanotube and conducting polymer composites for supercapacitors, Prog. Nat. Sci. 18 (2008) 777–788.
[3] Q. Yang, S.-K. Pang, K.-C. Yung, Study of PEDOT–PSS in carbon nanotube/conducting polymer composites as supercapacitor electrodes in aqueous solution, J. Electroanal. Chem. 728 (2014) 140–147.
[4] E. Frackowiak, K. Metenier, V. Bertagna, F. Beguin, Supercapacitor electrodes from multiwalled carbon nanotubes, Appl. Phys. Lett. 77 (2000) 2421–2423.
[5] W. Ma, C. Yang, X. Gong, K. Lee, A.J. Heeger, Thermally stable, efficient polymer solar cells with nanoscale control of the interpenetrating network morphology, Adv. Funct. Mater. 15 (2005) 1617–1622.
[6] M. Hokazono, H. Anno, N. Toshima, Thermoelectric properties and thermal stability of PEDOT:PSS films on a polyimide substrate and application in flexible energy conversion devices, J. Electron. Mater. 43 (2014) 2196–2201.
[7] G.A. Snook, P. Kao, A.S. Best, Conducting-polymer-based supercapacitor devices and electrodes, J. Power Sources 196 (2011) 1–12.
[8] R.A. Fisher, M.R. Watt, W. Jud Ready, Functionalized carbon nanotube supercapacitor electrodes: a review on pseudocapacitive materials, ECS J. Solid State Sci. Technol. 2 (2013) M3170–M3177.
[9] F.-J. Liu, Electrodeposition of manganese dioxide in three-dimensional poly(3,4-ethylenedioxythiophene)–poly(styrene sulfonic acid)–polyaniline for supercapacitor, J. Power Sources 182 (2008) 383–388.
[10] R. Jalili, J.M. Razal, G.G. Wallace, Exploiting high quality PEDOT:PSS–SWNT composite formulations for wet-spinning multifunctional fibers, J. Mater. Chem. 22 (2012) 25174–25182.
[11] E. Frackowiak, V. Khomenko, K. Jurewicz, K. Lota, F. Béguin, Supercapacitors based on conducting polymers/nanotubes composites, J. Power Sources 153 (2006) 413–418.
[12] S.K. Swain, I. Jena, Polymer/carbon nanotube nanocomposites: a novel material, Asian J. Chem. 22 (2010) 1–15.
[13] Q. Xiao, X. Zhou, The study of multiwalled carbon nanotube deposited with conducting polymer for supercapacitor, Electrochim. Acta 48 (2003) 575–580.
[14] B. Ding, X. Lu, C. Yuan, S. Yang, Y. Han, X. Zhang, Q. Che, One-step electrochemical composite polymerization of polypyrrole integrated with functionalized graphene/carbon nanotubes nanostructured composite film for electrochemical capacitors, Electrochim. Acta 62 (2012) 132–139.
[15] Z. Gao, W. Yang, J. Wang, B. Wang, Z. Li, Q. Liu, M. Zhang, L. Liu, A new partially reduced graphene oxide nanosheet/polyaniline nanowafer hybrid as supercapacitor electrode material, Energy Fuel 27 (2013) 568–575.
[16] D. Sun, X. Yan, J. Lang, Q. Xue, High performance supercapacitor electrode based on graphene paper via flame-induced reduction of graphene oxide paper, J. Power Sources 222 (2013) 52–58.
[17] L. Wang, G. Mu, C. Tian, L. Sun, W. Zhou, T. Tan, H. Fu, In situ intercalating expandable graphite for mesoporous carbon/graphite nanosheet composites as high-performance supercapacitor electrodes, ChemSusChem 5 (2012) 2442–2450.
[18] Z. Peng, D. Zhang, L. Shi, T. Yan, High performance ordered mesoporous carbon/carbon nanotube composite electrodes for capacitive deionization, J. Mater. Chem. 22 (2012) 6603–6612.
[19] D. Yu, K. Goh, L. Wei, H. Wang, Q. Zhang, W. Jiang, R. Si, Y. Chen, Multifunctional nitrogen-rich "brick-and-mortar" carbon as high performance supercapacitor electrodes and oxygen reduction electrocatalysts, J. Mater. Chem. A 1 (2013) 11061–11069.
[20] H. Wang, L. Shi, T. Yan, J. Zhang, Q. Zhong, D. Zhang, Design of graphene-coated hollow mesoporous carbon spheres as high performance electrodes for capacitive deionization, J. Mater. Chem. A 2 (2014) 4739–4750.
[21] A. Alabadi, X. Yang, Z. Dong, Z. Li, B. Tan, Nitrogen-doped activated carbons derived from a co-polymer for high supercapacitor performance, J. Mater. Chem. A 2 (2014) 11697–11705.
[22] J. Mi, X.-R. Wang, R.-J. Fan, W.-H. Qu, W.-C. Li, Coconut-shell-based porous carbons with a tunable micro/mesopore ratio for high-performance supercapacitors, Energy Fuel 26 (2012) 5321–5329.
[23] S. Nagamuthu, S. Vijayakumar, G. Muralidharan, Synthesis of Mn3O4/amorphous carbon nanoparticles as electrode material for high performance supercapacitor applications, Energy Fuel 27 (2013) 3508–3515.
[24] H. Li, J. Wang, Q. Chu, Z. Wang, F. Zhang, S. Wang, Theoretical and experimental specific capacitance of polyaniline in sulfuric acid, J. Power Sources 190 (2009) 578–586.
[25] C. Du, N. Pan, High power density supercapacitor electrodes of carbon nanotube films by electrophoretic deposition, Nanotechnology 17 (2006) 5314.
[26] X. Xie, L. Gao, Characterization of a manganese dioxide/carbon nanotube composite fabricated using an in situ coating method, Carbon 45 (2007) 2365–2373.
[27] J. Zhang, L.-B. Kong, H. Li, Y.-C. Luo, L. Kang, Synthesis of polypyrrole film by pulse galvanostatic method and its application as supercapacitor electrode materials, J. Mater. Sci. 45 (2010) 1947–1954.
[28] Q. Wang, L. Jiao, H. Du, Y. Si, Y. Wang, H. Yuan, Co_3S_4 hollow nanospheres grown on graphene as advanced electrode materials for supercapacitors, J. Mater. Chem. 22 (2012) 21387–21391.
[29] S.S. Zhang, K. Xu, T.R. Jow, EIS study on the formation of solid electrolyte interface in Li-ion battery, Electrochim. Acta 51 (2006) 1636–1640.
[30] H. Kurig, A. Jänes, E. Lust, Electrochemical characteristics of carbide-derived carbon|1 -ethyl-3-methylimidazolium tetrafluoroborate supercapacitor cells, J. Electrochem. Soc. 157 (2010) A272–A279.
[31] P.L. Taberna, P. Simon, J.F. Fauvarque, Electrochemical characteristics and impedance spectroscopy studies of carbon–carbon supercapacitors, J. Electrochem. Soc. 150 (2003) A292–A300.
[32] A. Laheäär, S. Delpeux-Ouldriane, E. Lust, F. Béguin, Ammonia treatment of activated carbon powders for supercapacitor electrode application, J. Electrochem. Soc. 161 (2014) A568–A575.
[33] E. Vitoratos, S. Sakkopoulos, E. Dalas, N. Paliatsas, D. Karageorgopoulos, F. Petraki, S. Kennou, S.A. Choulis, Thermal degradation mechanisms of PEDOT:PSS, Org. Electron. 10 (2009) 61–66.
[34] Y. Liu, C. Pan, J. Wang, Raman spectra of carbon nanotubes and nanofibers prepared by ethanol flames, J. Mater. Sci. 39 (2004) 1091–1094.
[35] N. Dementev, S. Osswald, Y. Gogotsi, E. Borguet, Purification of carbon nanotubes by dynamic oxidation in air, J. Mater. Chem. 19 (2009) 7904–7908.
[36] S. Hussain, R. Amade, E. Jover, E. Bertran, Functionalization of carbon nanotubes by water plasma, Nanotechnology 23 (2012) 8.
[37] I.D. Rosca, F. Watari, M. Uo, T. Akasaka, Oxidation of multiwalled carbon nanotubes by nitric acid, Carbon 43 (2005) 3124–3131.
[38] J. Zhang, H. Zou, Q. Qing, Y. Yang, Q. Li, Z. Liu, X. Guo, Z. Du, Effect of chemical oxidation on the structure of single-walled carbon nanotubes, J. Phys. Chem. B 107 (2003) 3712–3718.
[39] P. Tehrani, A. Kanciurzewska, X. Crispin, N.D. Robinson, M. Fahlman, M. Berggren, The effect of pH on the electrochemical over-oxidation in PEDOT:PSS films, Solid State Ionics 177 (2007) 3521–3527.
[40] J. Shen, A. Liu, Y. Tu, G. Foo, C. Yeo, M.B. Chan-Park, R. Jiang, Y. Chen, How carboxylic groups improve the performance of single-walled carbon nanotube electrochemical capacitors? Energy Environ. Sci. 4 (2011) 4220–4229.
[41] Y. Qin, J. Lu, P. Du, Z. Chen, Y. Ren, T. Wu, J.T. Miller, J. Wen, D.J. Miller, Z. Zhang, K. Amine, In situ fabrication of porous-carbon-supported [small alpha]-MnO2 nanorods at room temperature: application for rechargeable Li–O_2 batteries, Energy Environ. Sci. 6 (2013) 519–531.
[42] H.-S. Park, S.-J. Ko, J.-S. Park, J.Y. Kim, H.-K. Song, Redox-active charge carriers of conducting polymers as a tuner of conductivity and its potential window, Sci. Rep. 3 (2013).
[43] H. Ling, J. Lu, S. Phua, H. Liu, L. Liu, Y. Huang, D. Mandler, P.S. Lee, X. Lu, One-pot sequential electrochemical deposition of multilayer poly(3,4-ethylenedioxythiophene):poly(4-styrenesulfonic acid)/tungsten trioxide hybrid films and their enhanced electrochromic properties, J. Mater. Chem. A 2 (2014) 2708–2717.
[44] D.B. Mawhinney, V. Naumenko, A. Kuznetsova, J.T. Yates Jr., J. Liu, R.E. Smalley, Surface defect site density on single walled carbon nanotubes by titration, Chem. Phys. Lett. 324 (2000) 213–216.
[45] Y. Xiao, J.-Y. Lin, S.-Y. Tai, S.-W. Chou, G. Yue, J. Wu, Pulse electropolymerization of high performance PEDOT/MWCNT counter electrodes for Pt-free dye-sensitized solar cells, J. Mater. Chem. 22 (2012) 19919–19925.